scientific reports

Check for updates

OPEN

Pressure-dependent structural, mechanical, and electronic properties of XAu (X = Er, Tm) intermetallic compounds from first-principles calculations

A. Benmakhlouf[1], R. Mezouar[1,2], S. Daoud[1], M. A. Ghebouli[3,4], M. Fatmi[3]✉, K. Bouferrache[3,5], A. Djemli[4,6], Mustafa Jaipallah Abdelmageed Abualreish[7], Aseel Smerat[8], S. Alomairy[9,10] & Murat Yaylacı[11,12]

First-principles calculations of the structural parameters, elastic constants, mechanical moduli, Debye temperature, and density of states (DOS) of cubic CsCl-type (B2) XAu (X = Er, Tm) rare-earth intermetallic compounds under hydrostatic compression up to 20 GPa have been performed. The calculations were carried out within the framework of density functional theory (DFT) using the pseudopotential plane-wave (PP-PW) method and the local density approximation (LDA). The calculated elastic constants indicate that both ErAu and TmAu with the CsCl-type (B2) phase satisfy the Born mechanical stability criteria at equilibrium and under pressure up to 20 GPa for ErAu and up to about 19 GPa for TmAu. The zero-pressure structural parameters, elastic constants, and mechanical moduli are generally in good agreement with previously reported theoretical data. The calculated zero-pressure Young's modulus values are 96.61 GPa for ErAu and 73.94 GPa for TmAu, while the corresponding Debye temperatures are 193 K and 167 K, respectively. The obtained results reveal that hydrostatic pressure enhances the stiffness of both compounds, as reflected by the general increase in the elastic constants, acoustic wave velocities, and Debye temperature. Both ErAu and TmAu exhibit ductile behavior according to Pugh's ratio and show noticeable elastic anisotropy. The electronic-structure analysis confirms the metallic character of both compounds, while additional GGA + U calculations indicate that the localized 4f states are sensitive to the Hubbard correction without changing their metallic nature. The pressure-dependent elastic constants and related mechanical and thermodynamic properties of XAu (X = Er, Tm) intermetallic compounds have not been previously reported; therefore, the present results provide useful predictions and reference data for future theoretical and experimental studies.

Keywords Density functional theory (DFT), Intermetallic compounds, Rare-earth mono-aurides, Mechanical properties, Hydrostatic pressure, Density of states

[1]Laboratory of Materials and Electronic Systems (LMSE), University Mohamed El Bachir El Ibrahimi of Bordj Bou Arreridj, 34000 Bordj Bou Arreridj, Algeria. [2]Institute of Optics and Precision Mechanics, Ferhat Abbas University of Setif 1, 19000 Setif, Algeria. [3]Research Unit on Emerging Materials (RUEM), University Ferhat Abbas of Setif 1, 19000 Setif, Algeria. [4]Department of Chemistry, Faculty of Sciences, University of M'sila, 28000 University Pole, Road Bourdj Bou Arreiridj, M'sila, Algeria. [5]Department of Physics, Faculty of Sciences, University of M'sila, 28000 University Pole, Road Bourdj Bou Arreiridj, M'sila, Algeria. [6]Physics and Chemistry of Materials Lab, Faculty of Sciences, University of M'sila, 28000 University Pole, Road Bourdj Bou Arreiridj, M'sila, Algeria. [7]Department of Chemistry, college of Sciences, Northern Border University, P.O. Box 1321, 91431 Arar, Saudi Arabia. [8]Hourani Center for Applied Scientific Research, Al-Ahliyya Amman University, Amman 19328, Jordan. [9]Department of Physics, College of Science, Taif University, P.O.Box 11099, 21944 Taif, Saudi Arabia. [10]Department of Physics, College of Khurma University College, Taif University, P.O. Box 11099, Taif 21944, Saudi Arabia. [11]Department of Civil Engineering, Recep Tayyip Erdogan University, 53100 Rize, Türkiye. [12]Turgut Kıran Maritime Faculty, Recep Tayyip Erdogan University, 53900 Rize, Türkiye. ✉email: fatmimessaoud@yahoo.fr

Intermetallic compounds (IMCs) constitute a distinct class of materials that generally combine metallic and ceramic characteristics, such as high strength, high stiffness, good thermal stability, and complex bonding. These characteristics make this class of materials particularly relevant for fundamental research and advanced technological applications[1]. Among intermetallic compounds, rare-earth mono-aurides Ln-Au (Ln = Ce, Pr, Nd, Gd, Tb, Dy, Ho, Er, Tm, Yb, and Lu) have attracted considerable attention because of their high strength, very high melting points, high stiffness, good ductility, corrosion resistance, oxidation resistance, high-temperature mechanical performance, and good electrical properties[2].

High-temperature materials are essential for technologies operating under severe thermal and mechanical conditions, and gold-based rare-earth intermetallic have been considered promising candidates for such applications because of their remarkable physical and mechanical properties[3]. From the electronic point of view, previous first-principles investigations of REAu (RE = Tb, Ho, Er, Tm, and Yb) compounds showed their metallic character from density of states and band-structure analyses, and also indicated interesting thermoelectric behavior for some members of this family[4]. Experimentally, Chao et al. successfully synthesized CsCl-type phases of several gold- and silver-based rare-earth intermetallic compounds and showed that the unit-cell sizes of gold-based compounds are smaller than those of the corresponding silver-based alloys, suggesting stronger gold–rare-earth bonding[5]. Using the modified analytical embedded atom method, Wu et al. theoretically investigated the thermodynamic properties and lattice parameters of several RE-Au binary systems[6]. Saccone et al. studied the alloying behavior of Ho–Au, Er–Au, and Tm–Au systems using optical microscopy, scanning electron microscopy, X-ray diffraction, differential thermal analysis, and electron probe microanalysis techniques[7]. Meschel and Kleppa investigated the thermochemistry of binary alloys of gold with lanthanide metals by high-temperature direct synthesis calorimetry[8]. Kissell and Wallace reported the magnetic characteristics of some 1:1 compounds of lanthanides with gold and aluminum[9]. In addition, Gingerich and Finkbeiner determined the dissociation energies and predicted the stability of several gaseous rare-earth mono-aurides[10].

From the theoretical side, Ahamad et al. investigated strongly correlated rare-earth mono-aurides Ln-Au using first-principles calculations and reported their structural, elastic, and mechanical properties at zero pressure. Their work was based on the GGA-PBEsol approach[11] and the full-potential linearized augmented plane wave method implemented in the WIEN2k code[12]. However, to the best of our knowledge, there is no experimental or theoretical report in the literature on the pressure-dependent mechanical, thermodynamic, and electronic properties of XAu (X = Er, Tm) intermetallic compounds under hydrostatic compression. Recent ab initio studies have further confirmed the importance of first-principles approaches for describing structural, elastic, thermodynamic, electronic, and magnetic properties of intermetallic and related compounds. Benmakhlouf et al.[13] investigated cubic CsCl-type MgCa and showed that DFT calculations can provide reliable structural, elastic, and thermodynamic parameters for B2-type intermetallic systems. Bioud et al.[14] studied the thermodynamic and mechanical properties of B2-type CoTi and demonstrated the usefulness of elastic constants and Debye temperature in evaluating mechanical and thermal behavior. Zerrougui et al.[15] investigated FeX (X = Pt, Pd) phases and emphasized the importance of electronic and magnetic analyses in understanding metallic behavior and magnetic interactions. Chihi et al.[16] also combined experimental and theoretical approaches to study the structural, elastic, thermoelastic, and electronic properties of MO_3 (M = Cr, Fe, Al) compounds. These studies support the relevance of the present pressure-dependent investigation of structural, elastic, thermodynamic, and electronic properties of ErAu and TmAu intermetallic compounds. Recent first-principles studies have also demonstrated the importance of combining elastic, electronic, and phonon analyses for gold-based and B2-type intermetallic compounds. For instance, Al et al. investigated the mechanical and dynamical properties of X_3AuX (X = Ti, Zr, and V) gold-based compounds and showed that elastic stability and phonon spectra provide complementary information on the stability of these systems[17]. Similarly, Arikan and Bayhan studied the structural, electronic, and phonon properties of ZrRu and ZrZn in the B2 phase, emphasizing the usefulness of electronic band structures, density of states, and phonon dispersion in assessing metallicity and dynamical stability[18]. These studies further motivate the present investigation of the pressure-dependent structural, mechanical, and electronic properties of ErAu and TmAu in the CsCl-type B2 phase.

The present work aims to investigate the structural, elastic, mechanical, thermodynamic, and electronic properties of ErAu and TmAu intermetallic compounds in the cubic CsCl-type B2 phase under hydrostatic pressure up to 20 GPa. The pressure dependence of the elastic constants, mechanical stability, elastic anisotropy, acoustic wave velocities, Debye temperature, and electronic structure is systematically discussed.

Computational procedure

All first-principles calculations were performed within the (DFT) framework using the CASTEP software[19]. We adopted a plane-wave basis set and treated exchange-correlation (XC) interactions using the (LDA) parameterized by the Ceperley-Alder and Perdew-Zunger (CA-PZ) functional[20,21]. To reduce the plane-wave basis size, chemically inert core electrons were described via ultra-soft pseudopotentials[22]. The kinetic energy cutoff for the plane-wave expansion was set to 700 eV. Brillouin zone integration was performed using a Monkhorst-Pack[23] scheme with a 16 × 16 × 16 k-point grid. Full structural relaxation was carried out by optimizing the lattice parameters to minimize the total energy, atomic forces, and unit-cell stresses. Convergence criteria for the geometry optimization were established as follows: total energy variations below 5×10^{-6} eV/atom, maximum residual stress under 0.02 GPa, maximum ionic displacement below 5×10^{-4} Å, and Hellmann-Feynman forces restricted to 0.01 eV/Å.

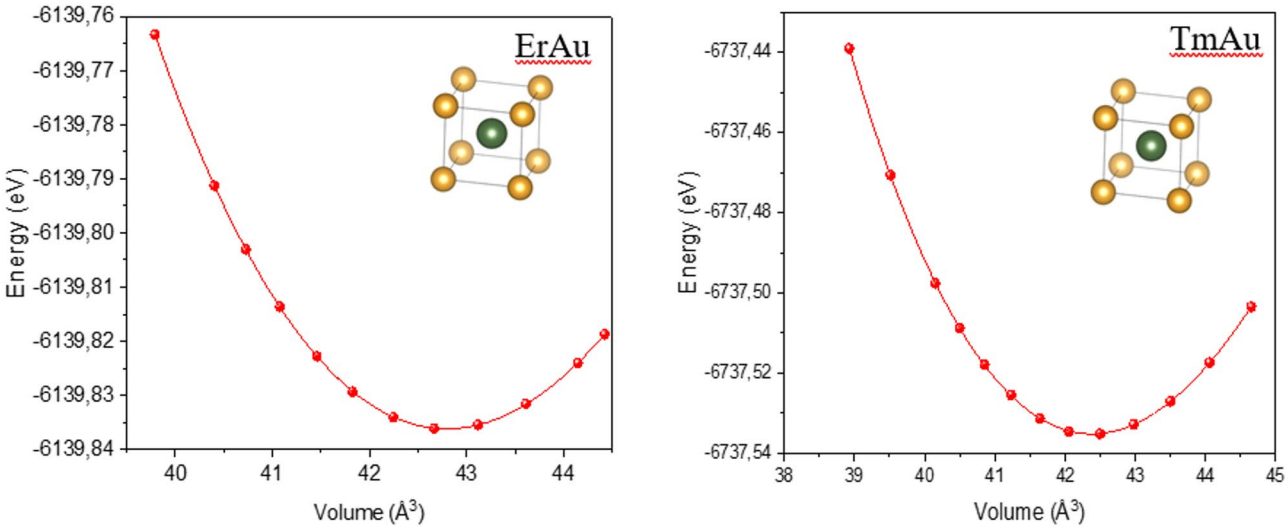


Fig. 1. Total energy as a function of unit-cell volume for ErAu and TmAu intermetallic compounds in the cubic CsCl-type B2 structure. The equilibrium structural parameters were obtained by fitting the energy–volume data using the Birch–Murnaghan equation of state.

Material	Method	a_0(Å)	B_0 (GPa)	B'_0	E_0 (eV)
ErAu	This work	3.49	96.97	4.26	− 6139.836
	Other works	3.51[a], 3.59[b], 3.5674[c], 3.527 [d], 3.52 [e], 3.569[f]			
TmAu	This work	3.48	92.43	4.80	− 6737.535
	Other works	3.50[a], 3.54 [b], 3.5459 [c], 3.516[d]			

Table 1. Lattice parameter a_0 (Å), bulk modulus B_0(GPa), its pressure derivative B'_0andminimum total energy E_0(eV) for both XAu (X = Er, Tm) materials, in comparison with other data of the literature[2,5,26]. [a]Ref[2]. (PBEsol-GGA), [b] Ref[2]. (PBE-GGA), [c] Ref[2]. (GGA + U), [d] Ref[5]. Experimental, [e] Ref[26]. EAM approach, [f] Ref[26]. VASP code.

Results and discussions

Structural properties

As we have mentioned in the abstract section, both ErAu and TmAu intermetallic compounds crystallize in cubic CsCl-type structure. To determine the equilibrium structural parameters, frequently both the total energy versus the volume of the unit cell (*E*-*V*) curve or data[13] and the pressure versus the unit cell volume (*P*-*V*) curve or data[24] have been used. The dependence of the total energy with the volume of the unit cell for both XAu (X = Er, Tm) materials is illustrated in Fig. 1. By fitting the (*E*-*V*) data illustrate in Fig. 1 with the Birch-Murnaghan's equation of state (BM-EOS)[25], we obtain four different equilibrium parameters, especially: the minimum total energy E_0, the bulk modulus B_0, the lattice parameter a_0, and the derivative of the bulk modulus with respect to pressure B'_0.Theexpression of the BM-EOS, which used here, is given as follows[13]:

$$E(V) - E_0 = \frac{9V_0B_0}{16}\left\{B'_0\left[\left(\frac{V_0}{V}\right)^{2/3} - 1\right]^3 + \left[\left(\frac{V_0}{V}\right)^{2/3} - 1\right]^2\left[6 - 4\left(\frac{V_0}{V}\right)^{2/3}\right]\right\} \quad (1)$$

where, V_0 is the equilibrium volume of the unit-cell, whileE_0 is the minimum total energy.

Our calculated values of the equilibrium lattice parametera_0, bulk modulus B_0 and its pressure derivative B'_0 as well as the minimum total energy $E_0$for both XAu (X = Er, Tm) materials are summarized in Table 1, along other theoretical data[2,26] and experimental values[5] of the literature.

There is strong evidence that our calculated values of a_0 coincide well with other theoretical data[2,22] and experimental values[5] of the literature. The deviation between our value (3.49 Å) of the lattice parametera_0 and the experimental one (3.527 Å) reported by Chao et al.[4] for ErAu intermetallic compound, and between our value (3.48 Å) of the a_0 and the experimental one (3.527 Å) reported by Chao et al.[5] for TmAu material is less than 1.1%. Note that the LDA approach gives lower values for the lattice parameter than both those obtained from the experience and the GGA approach[13].

Figure 2 shows the variation of the volume V of the unit-cell as a function of the applied hydrostatic pressure up to 20 GPa for both ErAu and TmAu materials. It is observed that the volume V of both ErAu and TmAu intermetallic compounds decreases monotonically with applied pressure up to 20 GPa. The decreasing of the volume V for both materials is a consequence of decreasing of the bond-length under elevated pressure.

To provide a quantitative description of this compression effect, the relative volume reduction was estimated from the calculated pressure-volume data. For ErAu, the unit-cell volume decreases from about 42.5 $Å^3$ at 0 GPa to about 36.9 $Å^3$ at 20 GPa, corresponding to a reduction of approximately 13%. For TmAu, the volume decreases from about 42.1 $Å^3$ to about 36.5 $Å^3$ over the same pressure range, giving a similar reduction of about 13%. This comparable compressibility behavior indicates that both compounds respond similarly to hydrostatic pressure, which is expected because they crystallize in the same B2 CsCl-type structure and contain neighboring rare-earth elements. The volume contraction reflects the shortening of the Er–Au and Tm–Au bond lengths under pressure, leading to stronger interatomic interactions and, consequently, increased elastic stiffness.

Mechanical properties

Determining elastic constants provides a robust benchmark for evaluating theoretical models[27]. It is widely recognized that density functional theory (DFT) based first-principles calculations yield highly accurate predictions for the elastic behavior of inorganic materials[28]. Moreover, characterizing these elastic and mechanical features provides essential insights into fundamental macroscopic thermal parameters, including specific heat, thermal expansion coefficients, Debye temperatures, and melting points[28]. Contemporary first-principles frameworks have advanced to a level of precision where they can reliably predict the physical properties of materials prior to experimental synthesis, as well as accurately reproduce existing empirical data[27]. Cubic crystals are governed by three independent elastic constants: C_{11}, C_{12}, and C_{44}[29]. Consequently, the bulk modulus B is derived using the relation B = (C11 + 2C12)/3[28,29]. The calculated elastic constants Cij and bulk moduli B for the ErAu and TmAu intermetallic compounds are presented in Table 2, alongside comparative theoretical values from the literature[2].

As we see, there are differences between our elastic constants calculated using the PP-PW method combined with the LDA approach, and these reported by Ahamad and co-workers[2], who have used the FP-LAPW method within GGA-PBE-sol. As a consequence, it can be said that the differences between the outcomes are due to different calculation techniques used in each work. The melting temperature Tm is a critical thermal parameter for evaluating solids in high-temperature applications[30]. For numerous cubic solids, Tm strongly correlates with the bulk modulus B through the empirical linear relationship Tm = 9.3B + 607[31], where Tm is given in K and B in GPa. By substituting our determined zero-pressure bulk moduli (B0 = 91.59 GPa for ErAu and 86.26 GPa for TmAu) into this equation, we estimate the melting points of the ErAu and TmAu intermetallic compounds to be 1458.8 K and 1409.2 K, respectively. These theoretical estimates are notably lower than the experimental values documented in established phase diagrams, which report 1710 K for ErAu and 1720 K for TmAu[7]. Furthermore,

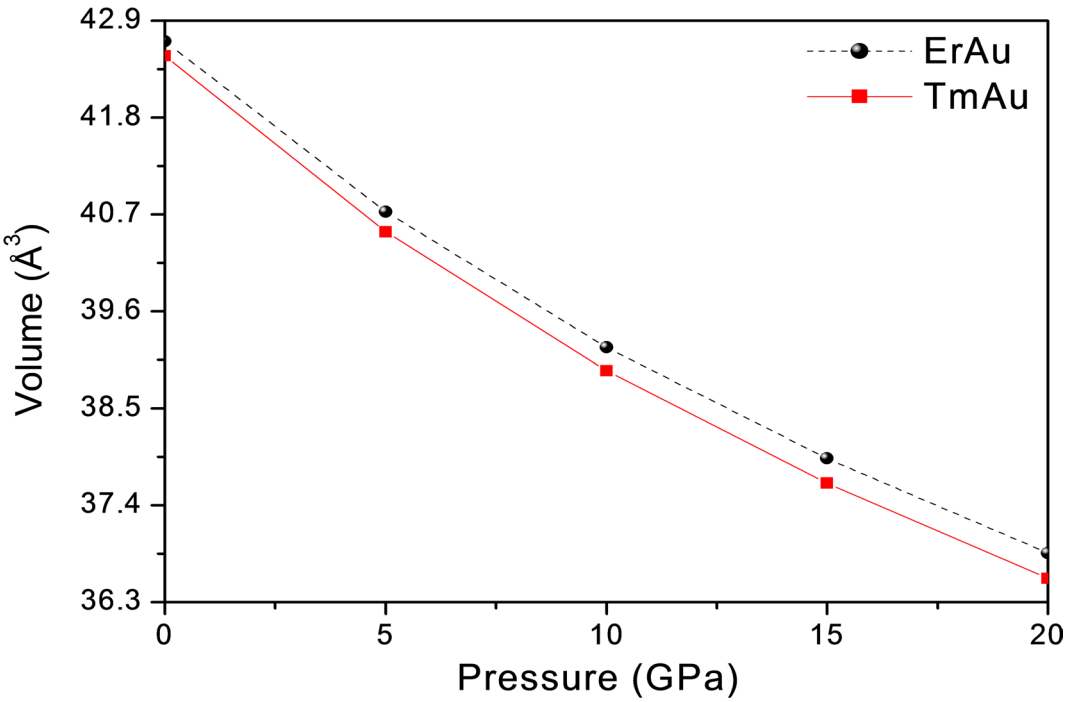


Fig. 2. Pressure dependence of the unit-cell volume of ErAu and TmAu intermetallic compounds in the CsCl-type B2 phase up to 20 GPa. The monotonic decrease in volume reflects the compression-induced shortening of Er–Au and Tm–Au bond lengths.

Material	Method	C_{11}	C_{12}	C_{44}	B
ErAu	This work	130.20	72.29	42.58	91.59
	Other work[2]	81.73	39.37	31.02	53.49
TmAu	This work	105.68	76.55	41.37	86.26
	Other work[2]	91.21	51.76	30.80	64.91

Table 2. Elastic constants (GPa)of for both ErAu and TmAu intermetallic compounds, along other theoretical data of the literature[2].

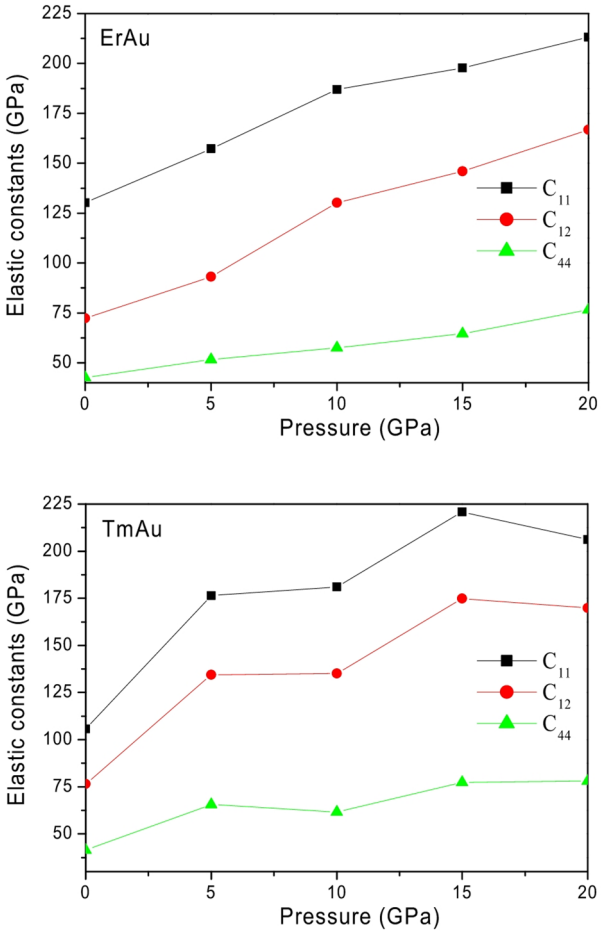


Fig. 3. Pressure dependence of the independent elastic constants C_{11}, C_{12}, and C_{44} for cubic ErAu and TmAu intermetallic compounds up to 20 GPa. The results show the evolution of the elastic response under hydrostatic compression.

to elucidate the impact of hydrostatic pressure on the mechanical stability of these intermetallic, we evaluated the independent elastic constants C11, C12, and C44 at pressures up to 20 GPa. The resulting pressure dependence of these elastic constants for both ErAu and TmAu crystals is illustrated in Fig. 3.

The elastic constants C_{11} and C_{12} exhibit closely parallel growth trends with rising pressure, whereas C_{44} responds differently, demonstrating a substantially weaker sensitivity to hydrostatic compression. Overall, the evaluated constants C_{11}, C_{12}, and C_{44} display a non-linear dependence on applied pressure. In the presence of external hydrostatic stress, the mechanical stability conditions for cubic crystals are modified to the following[32,33]:

$$K = \frac{1}{3}\left(C_{11} + 2C_{12} + p\right) \succ 0 \tag{2}$$

$$G = \frac{1}{2}\left(C_{11} - C_{12} - 2p\right) \succ 0 \tag{3}$$

$$G' = C_{44} - p \succ 0 \tag{4}$$

As shown in Fig. 4, our results indicate that both ErAu and TmAu intermetallic compounds with CsCl-type phase satisfy the Born stability criteria at equilibrium and under high pressure up to 20 GPa for ErAu and up to ~ 19 GPa for TmAu compound, respectively.

It should be emphasized that the Born stability criteria provide information only about the mechanical stability of the crystal against homogeneous elastic deformations. These criteria do not prove the full dynamical stability of the structure, which requires phonon-dispersion calculations and the absence of imaginary phonon frequencies throughout the Brillouin zone. Therefore, the present results confirm the mechanical stability of the B2 phase of ErAu and TmAu within the investigated pressure range, while the dynamical stability under pressure remains to be verified by future phonon calculations. This distinction between mechanical and dynamical stability is consistent with previous first-principles investigations. Al et al.[17] showed that, for X_3AuX gold-based compounds, elastic stability criteria should be complemented by phonon spectra to confirm dynamical stability. Similarly, Arikan and Bayhan[18] demonstrated that phonon-dispersion calculations are essential for confirming the dynamical stability of B2-type intermetallic systems. Therefore, although the present Born criteria confirm the mechanical stability of ErAu and TmAu under pressure, future phonon calculations are required to fully verify their dynamical stability.

As shown in Fig. 4, we find that the stability criterion G decreases gradually with the pressure and vanishes at about 19 GPa for TmAu intermetallic compound. Unfortunately, to the best of our knowledge, there are no other theoretical or measured data available in the literature on the Born stability criteria to compare with our results. The stiffness of a material structure can be investigated by calculating the polycrystalline elastic moduli[34]. For more details on the formulae describe the calculation details.

regarding these moduli for cubic crystals, please see for example[28,29]. The calculated values of the bulk modulus B, shear modulus G, Young's modulus E, Pugh's ratio B/G, and Poisson ratio σ of both ErAu and TmAu intermetallic compounds are given in Table 3, along other data of the literature[2]. The Pugh's ratio B/G informs on the ductility and the brittleness of the crystal. Smaller value of B/G imply brittleness, the critical value which makes a distinction between ductility and brittleness is 1.75[28]. The values of the B/G ratio are more than 1.75 for both ErAu and TmAu intermetallic compounds in all the range of hydrostatic pressure considered in

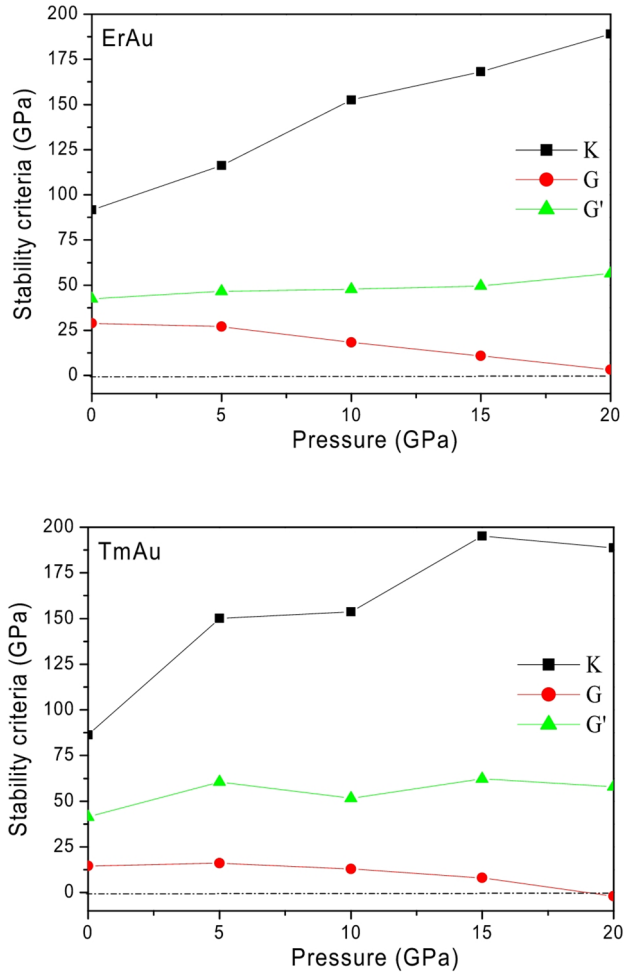


Fig. 4. Pressure dependence of the modified Born mechanical stability criteria K, G, and G′ for ErAu and TmAu intermetallic compounds in the CsCl-type B2 phase. Positive values indicate mechanical stability under hydrostatic pressure.

Material	*p* (GPa)	B(GPa)	G(GPa)	E(GPa)	B/G	σ	A
ErAu	0	91.59, 53.49 [a]	36.48,26.63[a]	96.61,69.53[a]	2.51,2.01[a]	0.32, 0.28 [a]	1.47, 1.465 [a]
	5	114.48	42.65	113.82	2.68	0.33	1.61
	10	149.11	43.37	118.61	3.44	0.37	2.03
	15	163.19	44.76	123.03	3.65	0.37	2.49
	20	182.28	47.49	131.09	3.84	0.38	3.31
TmAu	0	86.26, 64.91[a]	27.24, 25.76 [a]	73.94, 69.67 [a]	3.17,2.52[a]	0.36,0.32[a]	2.84, 1.562 [a]
	5	148.44	41.62	114.19	3.57	0.37	3.13
	10	150.38	41.53	114.09	3.62	0.37	2.68
	15	190.22	47.65	131.93	3.99	0.38	3.37
	20	182.00	43.80	121.64	4.16	0.39	4.32

Table 3. Elastic moduli, Pugh ratio (*B*/*G*), Poisson's ratio σ, and anisotropic factor *A* versus pressure *p* up to 20GPa for both ErAu and TmAu intermetallic compounds[2]. [a]Ref[2].

Table 3. Therefore, both ErAu and TmAu intermetallic compounds must be classified as ductile materials and possessing good plasticity. In order to increase the mechanical strength of any material used in any application, it is necessary to know the elastic anisotropy properties of this material[35]. To quantify the elastic anisotropy of materials, we distinguish different anisotropy factors, such as universal anisotropy factor A_U, Chung-Buesem anisotropy factor A_C, and Zener anisotropy factor A[36]. For both ErAu and TmAu intermetallic compounds, The Zener anisotropy factor, A, was determined utilizing the relation $A = 2C_{44}/(C_{11} - C_{12})$[32,36]. Table 3 presents these evaluated factors for the intermetallic compounds ErAu and TmAu. In a perfectly isotropic crystal, A equal's unity; thus, any departure from this value signifies elastic anisotropy[27]. Furthermore, the extent of this deviation directly quantifies the degree of anisotropic behavior inherent to the crystalline structure[27]. From Table 3, we can observe that the anisotropy factor was obtained larger than 1($A > 1$) for both ErAu and TmAu intermetallic compounds, indicating thatboth ErAu and TmAu crystals are elastically anisotropicand stiffest along the < 111 > body diagonals.

For comparison with related rare-earth mono-aurides, Ahamad et al.[2] reported Zener anisotropy factors of 1.465 for ErAu and 1.562 for TmAu, while other Ln-Au compounds show values such as 1.128 for HoAu, 1.247 for LuAu, 1.035 for NdAu, and 0.999 for DyAu. These values indicate that most rare-earth mono-aurides are elastically anisotropic, whereas NdAu and DyAu are nearly isotropic. The present value obtained for ErAu (A = 1.47 A = 1.47 A = 1.47) agrees very well with the previously reported value, while TmAu shows a larger anisotropy factor (A = 2.84 A = 2.84 A = 2.84), indicating a stronger directional dependence of the elastic response. Under pressure, the anisotropy of both compounds increases further, reaching A = 3.31 A = 3.31 A = 3.31 for ErAu and A = 4.32 A = 4.32 A = 4.32 for TmAu at 20 GPa. This suggests that hydrostatic compression enhances the elastic anisotropy of these B2 rare-earth mono-aurides. Additionally, we employed the ELATE software tool[37] to generate two- and three-dimensional anisotropy contour maps for Young's modulus E, linear compressibility β, shear modulus G, and Poisson's ratio υ for the intermetallic compounds ErAu and TmAu (shown in Figs. 5 and 6, respectively). For a strictly isotropic material, the 3D representation of an elastic parameter, such as linear compressibility β, exhibits a perfectly spherical shape across all crystallographic directions. Consequently, the extent of elastic anisotropy within a crystal is quantified by how much its 3D surface deviates from this ideal spherical morphology[38]. Figures 5 and 6 provide clear visual evidence of the anisotropic nature of both ErAu and TmAu. Furthermore, the directional extremum (minimum and maximum) values for Young's modulus E, shear modulus G, and Poisson's ratio υ have been computed; these results are tabulated in Table 4.

The linear compressibility of ErAu and TmAu intermetallic compounds have been found to be $\beta_{max} = \beta_{min} = 3.6393 TPa^{-1}$ for ErAu and $3.8643 TPa^{-1}$ for TmAu, respectively. To the best of the authors' knowledge, there are no data available in the literature on the 2D and 3D anisotropy for both XAu (X = Er, Tm) materials. The lack of experimental and other theoretical results did not allow us to compare our results on the 2D and 3D anisotropy for both ErAu and TmAu compounds.

Debye temperature

The Debye temperature, θ_D, is a fundamental thermodynamic quantity that yields critical insights into the phonon spectrum of a crystal, thereby governing its thermal and electrical transport properties. Phonon wavelengths are characteristically short at temperatures exceeding θ_D, whereas they become significantly extended below this thermal threshold[30]. Typically, θ_D exhibits a positive correlation with applied pressure[39–41] and an inverse relationship with temperature[34,42,43]. For cubic systems crystallizing in a CsCl-type phase, θ_D can be evaluated using the average sound velocity, v_m, and the lattice parameter, a, according to the following expression[44]:

$$\theta_D = 375.1 \frac{\nu_m}{a} \tag{5}$$

where ν_m and a should be expressedin km/s and Å, respectively.

The average sound velocity ν_m may be calculated by performing a harmonic mean as follows[33,34]:

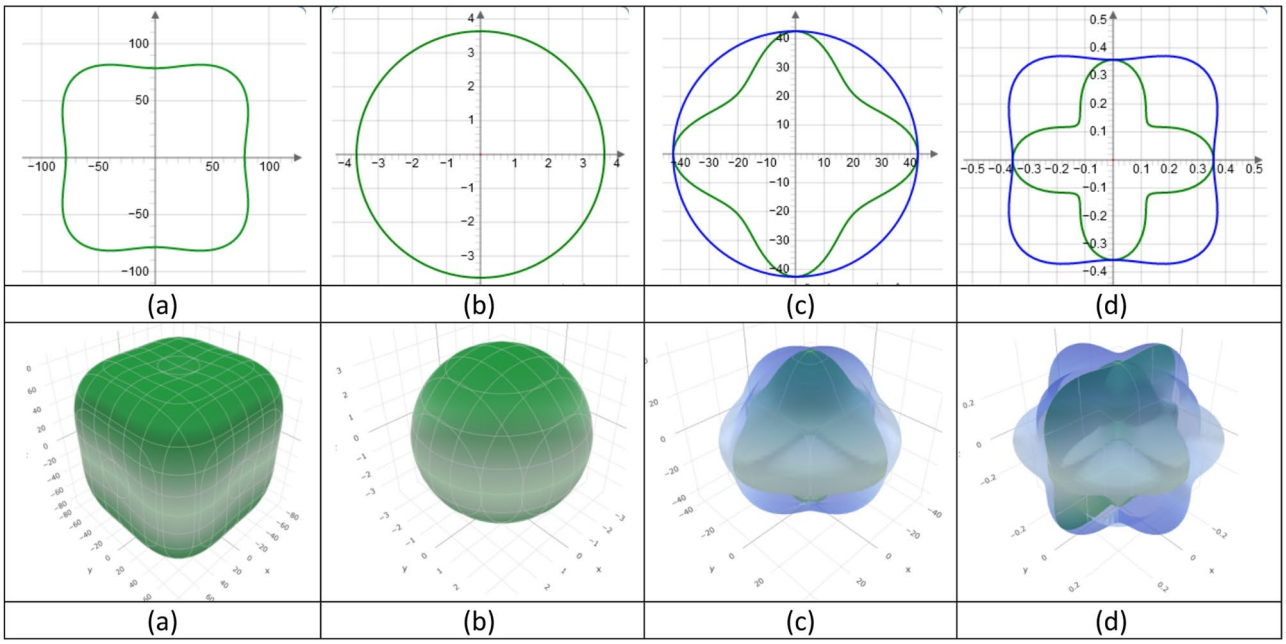


Fig. 5. Two-dimensional and three-dimensional anisotropy contour plots of ErAu, showing the directional dependence of (**a**) Young's modulus EEE, (**b**) linear compressibility β\betaβ, (**c**) shear modulus GGG, and (**d**) Poisson's ratio.

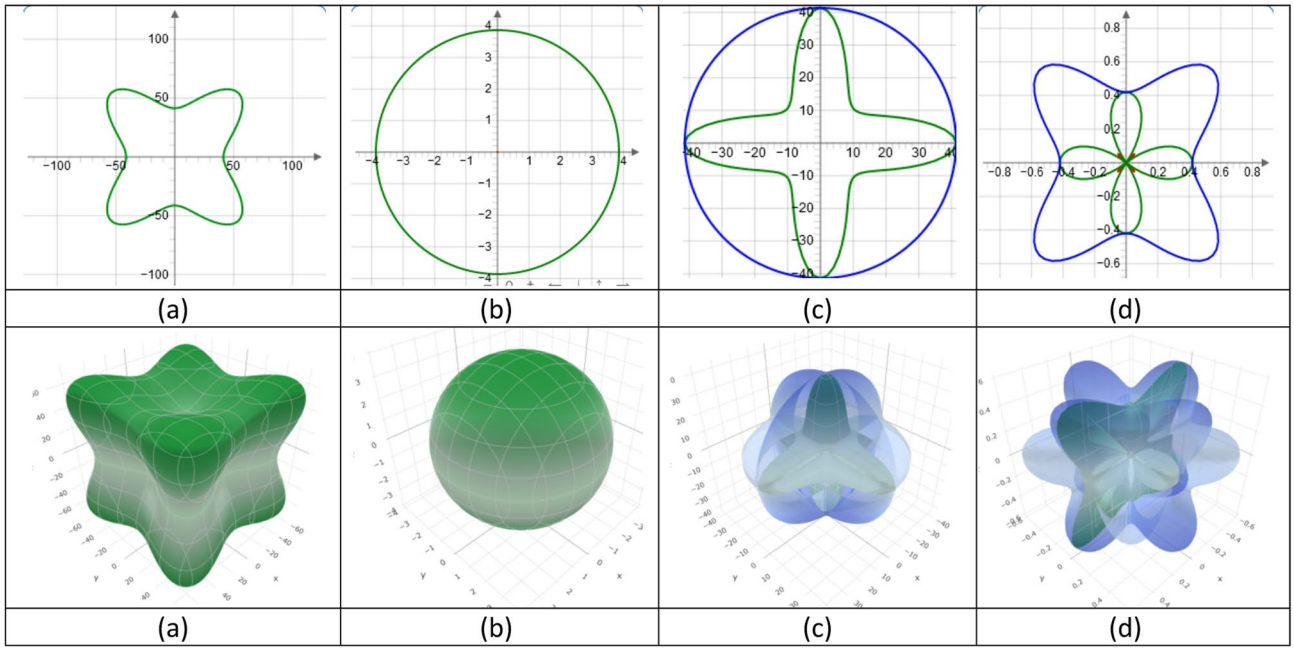


Fig. 6. Two-dimensional and three-dimensional anisotropy contour plots of TmAu, showing the directional dependence of (**a**) Young's modulus EEE, (**b**) linear compressibility β\betaβ, (**c**) shear modulus GGG, and (**d**) Poisson's ratio.

	E_{min}	E_{max}	G_{min}	G_{max}	υ_{min}	υ_{max}
ErAu	78.58	110.6	28.96	42.58	0.179	0.456
Anisotropy	1.41		1.47		2.55	
TmAu	41.367	107	14.565	41.37	−0.074	0.778
Anisotropy	2.587		2.84		∞	

Table 4. The min and max limits of young's modulus *E*, shear modulus *G*, and Poisson's ratio υ of both ErAu and TmAu intermetallic compounds.

Material	*p* (GPa)	v_l(km/s)	v_t (km/s)	v_m(km/s)	θ_D (K)
ErAu	0	3.145	1.604	1.798	193.0
		2.537 [a]	1.376[a]	1.535 [a]	129.3 [a]
		2.522 [b]	1.380 [b]	1.539 [b]	164.4 [b]
	5	3.397	1.695	1.901	207.3
	10	3.662	1.676	1.889	208.6
	15	3.739	1.675	1.890	211.0
	20	3.869	1.701	1.921	216.5
TmAu	0	2.928	1.380	1.553	167.0
		2.644 [a]	1.323 [a]	1.484 [a]	125.5 [a]
		2.646 [b]	1.348 [b]	1.511 [b]	161.9 [b]
	5	3.687	1.666	1.878	205.2
	10	3.631	1.631	1.840	203.6
	15	3.965	1.718	1.941	217.2
	20	3.804	1.624	1.835	207.4

Table 5. Longitudinal, transverse, and average acoustic wave velocities and Debye temperature versus pressure up to 20 GPa for ErAu and TmAu intermetallic compounds, compared with the wrong values reported in Ref[2]. and the correcte values. [a]Ref[2],[b]Ref[34].

$$v_m = \left[\frac{1}{3}\left(\frac{2}{v_t^3} + \frac{1}{v_l^3}\right)\right]^{-1/3} \tag{6}$$

where $v_l$and $v_t$are the longitudinal and transverse elasic wave speed, respectively. They are calculated from the following Equations[33,34]:

$$v_l = \left(\frac{3B + 4G}{3\rho}\right)^{1/2} \text{ and } v_t = \left(\frac{G}{\rho}\right)^{1/2} \tag{7}$$

where *B* is the bulk modulus *G* is the shear modulus, and ρ is the mass density, respectively.

Our obtained values of the longitudinal, transverse andmean acoustic wave speeds, and Debye temperature θ_D for both ErAu and TmAu intermetallic compounds are narrated in Table 5, along other data of the literature[2]. It is very important to note that all the values of both elastic wave velocities (v_l, v_t, andv_m) and Debye temperature $\theta_D$of both ErAu and TmAu intermetallic obtained Ahamad et al.[2] are not correct.At the same time, we have recalculated the correct values of v_l, v_t, v_m and θ_D for both ErAu and TmAu intermetallic compounds, based on the lattice parameter *a*and the elastic constants C_{ij} obtained by Ahamad et al.[2], and the corrected values are also reported in Table 5. The origin of the discrepancy in the Debye temperature values reported by Ahamad et al.[2]. is related mainly to the numerical use of the number of atoms in the Debye-temperature expression. In Ref[2]., the authors used $n = 1$ for the CsCl-type structure. However, the B2 CsCl-type unit cell of ErAu and TmAu contains two atoms per formula unit, namely one rare-earth atom and one Au atom. Therefore, $n = 2$ should be used in the Debye-temperature calculation. Using $n = 1$ underestimates θD by a factor of $2^{1/3}$. By using $n = 2$, together with the elastic constants, density, and sound velocities reported in Ref[2]., the corrected Debye temperatures listed in Table 5 are obtained. Therefore, the discrepancy is mainly due to a formula-unit/unit-cell counting issue in the Debye-temperature evaluation rather than an error in the elastic-wave velocity formulas.

The Debye temperature values (193 and 167 K) suggest moderate thermal stability of both ErAu and TmAu intermetallic compounds, making such materials suitable for medium-demand thermal and acoustic applications[45]. We observe that our values of both elastic wave velocities (v_l, v_t, andv_m) and Debye temperature $\theta_D$of both ErAu and TmAu intermetallics are in general higher than the theoretical data reported by Ahamad et al.[2]. The lack of other theoretical and experimental results did not allow us to compare our results. Nevertheless, we hope that our results can support further experiments. As shown in Table 4, all the acoustic wave speeds

and Debye temperature θ_D increase monotonously (except the fluctuation observed at p= 15GPa for TmAu intermetallic) but non-linearly with increasing pressure from 0 up to 20 GPa. Similarly, the Debye temperature increases also with increasing pressure for cubic perovskite $BaHfO_3$ under pressure up to 80 GPa[33], and for XThSn (X = Pt, Ni) thermoelectric materials[46].It can be noted that Debye temperature θ_D of both ErAu and TmAu intermetallic compounds are smaller than the value (413.7 K) of θ_D reported for NiThSn half-Heusler semiconducting compound[34], and vey smaller than the calculated value (991.9 K) of θ_D reported for perovskite-type $NaBeH_3$ hydride material[28].

Electronic structure: band structure, DOS and PDOS

The electronic properties of material play a dominant role on the relationship between the magnetic momentsand the stability of the structure[47]. Furthermore, the examination of the electronic density of states (DOS) at the Fermi level as a function of the volume helps on the determination of the electronic contribution to the heat capacity *Cp* in material[48]. Figure 7a and b show the total density of states (TDOS), which often describes the behavior of the band structures, and the partial density of states (PDOS), which evaluate the individual atom contributions to the TDOS, for both ErAu and TmAu intermetallic compounds. The PDOS of both ErAu and TmAu intermetallic com materials pounds exhibits non-zero values at Fermi level, which indicates the metallic feature of both compounds. For both materials XAu (X = Er, Tm), the density of states (Fig. 7a and b) is dominated by the Au 5d band in the − 6 to − 3 eV energy range and by the rare-earth 4f states near the Fermi level. This shows that the way they bond is similar in both and it is because of the Au 5d and rare earth 4f hybridization. The Au partial DOS is remarkably similar in both intermetalliccompounds, with the 5d band peaking at approximately − 4.9 eV in ErAu material and − 4.8 eV in TmAu compound, with comparable intensities of around 8.0–8.5 electrons/eV. This similarity confirms that the Au sublattice contributes a nearly unchanged electronic background across the two systems, and that the primary source of differentiation between ErAu intermetallic compound and TmAu material lies in the rare-earth 4f manifold.

To further examine the influence of localized rare-earth 4f electrons, additional GGA+U calculations were performed by applying an effective Hubbard parameter Ueff=6 eV to the Er-4f and Tm-4f states. The calculated band structures obtained using both GGA and GGA+U are shown in Fig. 8. The comparison indicates that the inclusion of the Hubbard correction mainly modifies the position and dispersion of the 4f-derived bands, confirming the sensitivity of the electronic structure to the treatment of localized 4f electrons. Nevertheless, several bands still cross the Fermi level in both compounds, demonstrating that the metallic character of ErAu and TmAu is preserved after the inclusion of the Hubbard correction.These additional GGA+U calculations were introduced to address the localized nature of the Er-4f and Tm-4f electrons and to provide a more reliable description of the 4f-derived electronic bands. The results show that the Hubbard correction affects mainly the rare-earth 4f states, while the metallic character remains unchanged. The most significant structural difference between the two DOS profiles concerns the energy position and distribution of the 4f states. TmAu intermetallic compound has a noticeable splitting of the 4f manifold into two sharp peaks at − 2.26 eV and − 0.09 eV (Fig. 7b). These peaks are almost the same size of ~ 13 electrons/eV. In ErAu intermetallic compound, the two peaks are not as symmetrical, the first one is at energy of ~ − 4.28 eV, while the second peakis positioned at energy of ~ − 0.09 eV. The difference between these peaks is about 4.2 eV. This is because the crystal field environments and exchange splitting strengths are different for ErAu material and TmAu intermetallic compound. TmAu material has one more 4f electron than ErAu compound. It can be noticed also that both compounds exhibit a large DOS at the Fermi level driven by the 4f states (Fig. 7a and b) suggests a stronger tendency toward magnetic ordering

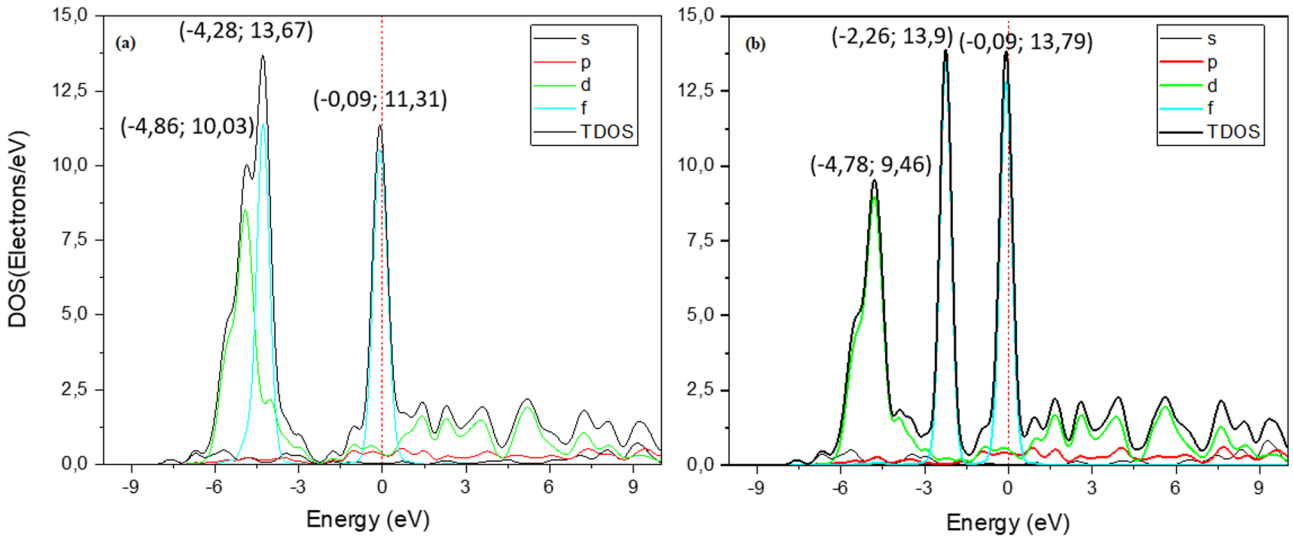


Fig. 7. Total density of states (TDOS) and partial density of states (PDOS) of (**a**) ErAu and (**b**) TmAu intermetallic compounds in the CsCl-type B2 structure. The Fermi level is set to 0 eV, and the main states near the Fermi level are dominated by rare-earth 4f contributions.

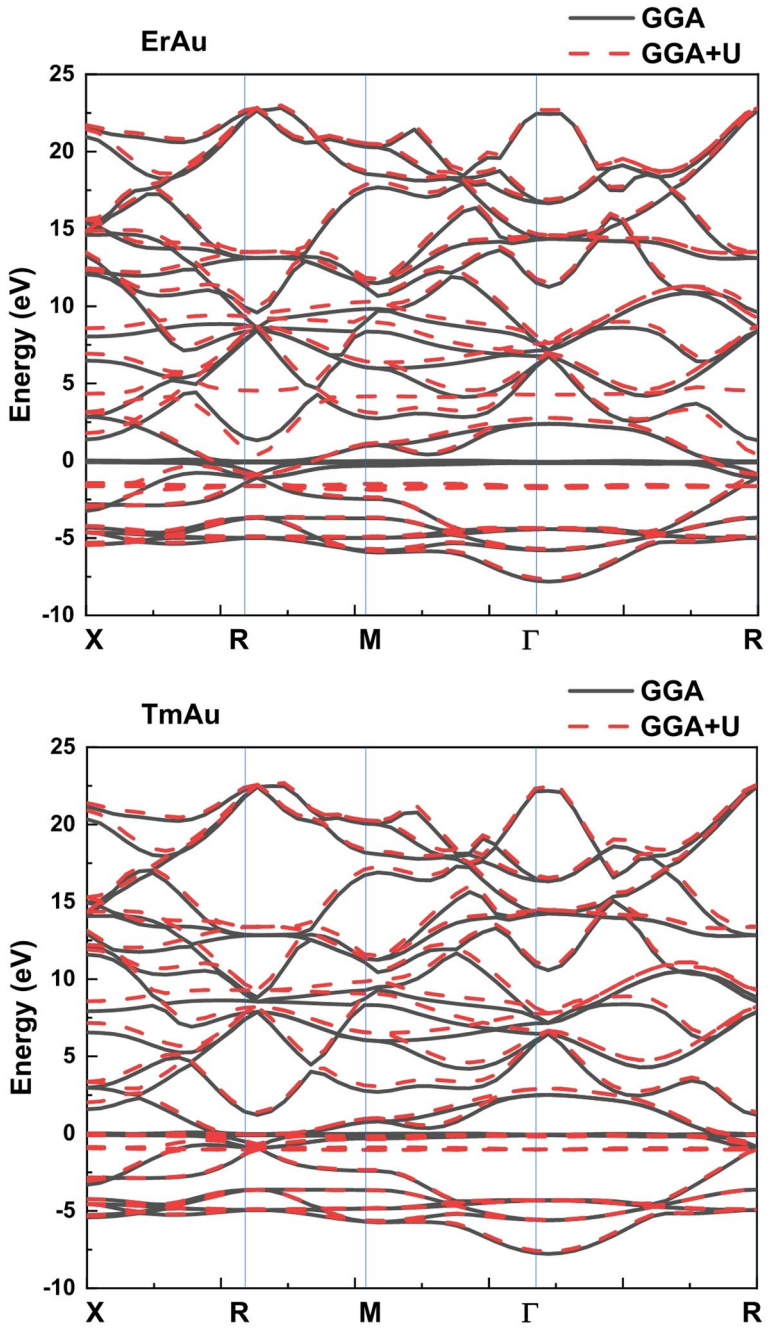


Fig. 8. Calculated electronic band structures of (**a**) ErAu and (**b**) TmAu in the B2 phase using GGA and GGA + U approaches. The Hubbard correction was applied to the localized Er-4f and Tm-4f states using Ueff = 6 eV. The Fermi level is set to 0 eV.

compared to ErAu intermetallic compound. However, the higher and more symmetric $N(E_F)$) observed in TmAu material (Fig. 7b) suggests a relatively stronger possible magnetic tendency compared to ErAu intermetallic compound. Nevertheless, this statement should be understood only as a qualitative indication based on the DOS profile. The Stoner-like argument alone is not sufficient to determine the true magnetic ground state or the local magnetic moments. In fact, the available Materials Project data for the B2 phases of ErAu and TmAu classify both compounds as non-magnetic metallic systems, with zero total magnetization. This supports the revised interpretation that the finite 4f contribution at the Fermi level should not be considered as direct evidence of a magnetic ground state.

It can also be noticed that both compounds exhibit a noticeable DOS at the Fermi level mainly driven by the rare-earth 4f states, as shown in Fig. 8a and b. This feature may qualitatively suggest a possible magnetic tendency within a Stoner-like picture. However, the present DOS results alone cannot be used to determine the true magnetic ground state or the local magnetic moments of these compounds. Therefore, dedicated spin-

polarized calculations are required for a rigorous magnetic assessment. In this context, the additional spin-polarized GGA + U calculations performed in the present revision provide a more appropriate treatment of the localized 4f states. The full simultaneous inclusion of spin-orbit coupling and DFT + U remains a limitation of the present computational setup and is proposed for future work.

Conclusion

we examine the effects of applied pressure up to 20 GPa on the structural characteristics, elastic constants, and related macroscopic properties of the intermetallic compounds ErAu and TmAu crystallized in the CsCl-type (B2) phase. Calculations were performed utilizing pseudopotential plane-wave formalism within the local density approximation (LDA). As pressure increases from 0 to 20 GPa, the elastic constants and derived thermodynamic parameters, including acoustic wave velocities and the Debye temperature (θD), exhibit a predominantly monotonic yet non-linear evolution, albeit with minor fluctuations. Evaluation of the Born stability criteria confirms that the B2 phase remains mechanically stable both at equilibrium and under compression up to approximately 20 GPa for ErAu and 19 GPa for TmAu. At ambient pressure, our LDA-derived elastic constants display slight deviations from the prior theoretical predictions. Additionally, analysis of the total and partial density of states (TDOS and PDOS) corroborates the intrinsic metallic character of both systems. Crucially, a pronounced density of states at the Fermi level, primarily driven by the 4f orbitals, implies that both ErAu and TmAu satisfy the Stoner criterion for magnetic instability.

Data availability

Data availability statement: Data underlying the results presented in this paper are not publicly available at this time but may be obtained from the corresponding author (fatmimessaud@yahoo.fr) upon reasonable request.

Received: 1 May 2026; Accepted: 10 June 2026
Published online: 23 June 2026

References

1. Mamatyusup, M., Wei, Q., Lin, Z., Luo, J. & Zhang, M. Pressure induced B2→ transition and metal–narrow bandgap semiconductor transition in CuSc intermetallic compound. *Phys. B*. **730**, 418461. https://doi.org/10.1016/j.physb.2026.418461 (2026).
2. Ahamad, S., Shafq, M., Ahamad, R., Asadabadi, S. J. & Ahamad, I. Strongly correlated intermetallic rare earth monoaurides (ln-Au): Ab-initio study. *J. Rare Earths* **36**, 1106–1111. https://doi.org/10.1016/j.jre.2018.03.018 (2018).
3. Ahamad, S., Ahamad, R. & Ahamad, I. Physical properties and possible applications of gold-based rare earth intermetallics (R-Au): A review. *J. Magn. Magn. Mater.* **490**, 165477. https://doi.org/10.1016/j.jmmm.2019.165477 (2019).
4. Ahamad, S., Ahamad, R., Bilal, M. & Rehman, N. U. DFT studies of thermoelectric properties of ReAuintermetallics at 300 K. *J. Rare Earths* **36**, 197–202. https://doi.org/10.1016/j.jre.2017.08.004 (2018).
5. Chao, C. C., Luo, H. L. & Duwez, P. CsCl type compounds in binary alloys of rare earth metals with gold and silver. *J. Appl. Phys.* **34** (7), 1971. https://doi.org/10.1063/1.1729720 (1963).
6. Wu, Y., Hu, W. & Han, S. Theoretical calculation of thermodynamic data for gold-rare earth alloys with the embedded-atom method. *J. Alloys Compd.* **420** (1), 83–93. https://doi.org/10.1016/j.jallcom.2005.10.020 (2006).
7. Saccone, A., Macciò, D., Delfino, S. & Ferro, R. Alloying behavior of the rare earth metals with gold: The Ho–Au, Er–Au and Tm–Au systems. *Intermetallics* **10** (9), 903–913. https://doi.org/10.1016/s0966-9795(02)00093-6 (2002).
8. Meschel, S. V. & Kleppa, O. J. Thermochemistry of some binary alloys of gold with the lanthanide metals by high temperature direct synthesis calorimetry. *J. Alloys Compd.* **363** (1–2), 242–247. https://doi.org/10.1016/S0925-8388(03)00527-9 (2004).
9. Kissell, F. & Wallace, W. Magnetic characteristics of some 1: 1 compounds of the lanthanides with gold and aluminum. *J. Less Common. Met.* **11** (6), 417–422. https://doi.org/10.1016/0022-5088(66)90088-9 (1966).
10. Gingerich, K. & Finkbeiner, H. Mass spectrometric determination of the dissociation energies of LaAu, CeAu, PrAu, and NdAu and predicted stability of gaseous monoaurides of electropositive metals. *J. Chem. Phys.* **52** (6), 2956–2964. https://doi.org/10.1063/1.1673424 (1970).
11. Perdew, J. P. et al. Restoring the density-gradient expansion for exchange in solids and surfaces. *Phys. Rev. Lett.* **100**, 136406. https://doi.org/10.1103/PhysRevLett.100.136406 (2008).
12. Blaha, P. et al. An Augmented Plane Wave þ Local Orbitals Program for Calculating Crystal Properties, K. Schwarz TechnicalUniversitat, Wien, Austria, ISBN 3-9501031-1-2 (2001).
13. Benmakhlouf, A. et al. Structural elastic and thermodynamic properties of cubic CsCl type MgCa using ab initio approach. *Sci. Rep.* **15**, 18781. https://doi.org/10.1038/s41598-025-03689-y (2025).
14. Bioud, N. et al. Computational investigation of thermodynamic and mechanical properties of B2-type CoTi intermetallic compound. *Phys. Solid State*. **67**, 68–74. https://doi.org/10.1134/S1063783424601760 (2025).
15. Zerrougui, Z. et al. Study of structural, elastic, mechanical, electronic and magnetic properties of FeX (X = Pt, Pd) austenitic and martensitic phases. *Solid State Sci.* **141**, 107211. https://doi.org/10.1016/j.solidstatesciences.2023.107211 (2023).
16. Chihi, T., Fatmi, M., Ghebouli, B. & Ghebouli, M. A. Structural, elastic, thermoelastic and electronic properties of M2O3 (M = Cr, Fe, Al) compounds: Experimental and theoretical study. *Results Phys.* **12**, 725–731. https://doi.org/10.1016/j.rinp.2018.12.034 (2019).
17. Al, S., Arikan, N., Özduran, M. & İyigör, A. Computational investigations of mechanical and dynamical properties of gold-based compounds (X3AuX_3AuX3Au, X = Ti, Zr and V). *Chin. J. Phys.* **56**, 1508–1514. https://doi.org/10.1016/j.cjph.2018.06.001 (2018).
18. Arikan, N. & Bayhan, Ü. Ab initio calculation of structural, electronic and phonon properties of ZrRu and ZrZn in B2 phase. *Phys. B: Condens. Matter*. **406**, 3234–3237. https://doi.org/10.1016/j.physb.2011.05.031 (2011).
19. Ghebouli, B., Ghebouli, M. A., Chihi, T., Fatmi, M. & Boucetta, S. M. Reffas,First-principles study of structural, elastic, electronic and optical properties of SrMO3 (M = Ti and Sn). *Solid State Commun.* **149** (47–48), 2244–2249. https://doi.org/10.1016/j.ssc.2009.09.001 (2009).
20. Benlakhdar, F. et al. Electronic and optical properties of lead-free $K_2AgSbBr_6$ double perovskite tuned by doping elements Cu^+, Bi^{3+}, and I^-. *Sci. Rep.* **15**, 40362. https://doi.org/10.1038/s41598-025-24417-6 (2025).
21. Bouferrache, K. et al. Synergistic optoelectronic and thermoelectric performance in $Rb_2AsAuBr_6$ and $Rb_2AsAuCl_6$ double perovskites for multifunctional energy conversion. *Sci. Rep.* **16**, 13616. https://doi.org/10.1038/s41598-026-42440-z (2026).
22. Vanderbilt, D. Soft self-consistent pseudopotentials in generalized eigenvalue formalism. *Phys. Rev. B*. **41**, 7892–7895. https://doi.org/10.1103/PhysRevB.41.7892 (1990).
23. Fatmi, M. et al. High performance double perovskites of $Cs_2InAgBr_6$ and $Cs_2InAgCl_6$ structural electronic optical and thermoelectric properties for next generation photovoltaics. *Sci. Rep.* **15**, 20851. https://doi.org/10.1038/s41598-025-04600-5 (2025).

24. Benamrani, A., Daoud, S. & Bouarissa, N. First principles study of structural, elastic and thermodynamic properties of $LiAl_2X$ (X = Rh, Pd, Ir and Pt) intermetallic compounds. *Eur. Phys. J.* **B95**, 106. 10.1140/ep jb/s10051-022-00370-5 (2022).
25. Birch, F. Finite elastic strain of cubic crystals. *Phys. Rev.* **71**, 809–824. https://doi.org/10.1103/PhysRev.71.809 (1947).
26. Wu, Y. R., Hu, W. Y. & Han, S. C. Theoretical calculation of thermodynamic data for gold-rare earth alloys with the embedded-atom method. *J. Alloys Compd.* **420** (1), 83–93. https://doi.org/10.1016/j.jallcom.2005.10.020 (2006).
27. Rached, D., Rabah, M., Khenata, R., Abidri, B. & Benalia, S. Structural phase transition and elastic properties of curium and uranium monobismuthides under pressure effect. *Solid State Commun.* **149**, 1772–1776. https://doi.org/10.1016/j.ssc.2009.07.033 (2009).
28. Rahrah, M., Lebga, N., Latreche, A. & Daoud, S. Pressure dependence of mechanical properties of perovskite-type hydride $NaBeH_3$ material: First principle calculations. *Bull. Mater. Sci.* **47**, 242. https://doi.org/10.1007/s12034-024-03320-2 (2024).
29. Rekab-Djabri, H. et al. Full-potential linear muffin-tin orbital investigation of the structural, electronic, elastic and optical properties of semiconducting $AgBr_{1-x}I_x$ ($0 \le x \le 1$) ternary alloys. *Can. J. Phys.* **98** (9), 834–848. https://doi.org/10.1139/cjp-2019-0357 (2020).
30. Durukan, I. K. & Ciftci, Y. O. First-principles study on B2 based XAl (X = Rh, Ru) compounds. *Phys. Scri.* **96**, 125726. https://doi.org/10.1088/1402-4896/ac3b6d (2021).
31. Fine, M. E. & Brown, L. D. Marcus, elastic constants versus melting temperature in metals. *Scr. Metall.* **18**, 951. https://doi.org/10.1016/0036-9748(84)90267-9 (1984).
32. Daoud, S., Bioud, N., Lebga, N., Belagraa, L. & Mezouar, R. Pressure effect on structural, elastic and electronic properties of (B3) BSb compound. *Indian J. Phys.* **87** (4), 355–361. https://doi.org/10.1007/s12648-012-0231-y (2013).
33. Gu, F., Chen, Y-Y., Zhang, X-L., Zhang, J-H. & Liu, Q-Q. First-principles calculations for the structural, elastic and thermodynamic properties of cubic perovskite $BaHfO_3$ under pressure. *Phys. Scr.* **89** (12pp), 105703. https://doi.org/10.1088/0031-8949/89/10/105703 (2014).
34. Ouledali, M. et al. Structural, mechanical, electronic, optical and vibrational Properties of NiThSn: DFT prediction,Cryst. *Res. Technol.* **61** (3), e70092. https://doi.org/10.1002/crat.70092 (2026).
35. Kars Durukan, İ. & ÖztekinÇiftci, Y. The effect of pressure on elastic anisotropy, vibration and optical properties of a AgScSi compound. *J. Electron. Mater.* **48**, 4050–4056. https://doi.org/10.1007/s11664-019-07167-w (2019).
36. Dabhi, V. A. & Patel, H. S. A. M. Vora,First principles investigation of the structural, anisotropic mechanical, optical, thermodynamic, and thermoelectric properties of MF_2 (M = Ca, Sr, Ba, Pb) florite minerals using density functional theory. *Next Mater.* **8**, 100893. https://doi.org/10.1016/j.nxmate.2025.100893 (2025).
37. Gaillac, R., Pullumbi, P. & Coudert, F-X. ELATE: an open-source online application for analysis and visualization of elastic tensors. *J. Phys. Condens. Matter.* **28**, 275201. https://doi.org/10.1088/0953-8984/28/27/275201 (2016).
38. Ahmed, T. et al. Physical properties of rare earth perovskites $CeMO_3$ (M = Co, Cu) in the context of density functional theory. *Mater. Today Commun.* **29**, 12. https://doi.org/10.1016/j.mtcomm.2021.102973 (2021).
39. Bioud, N. & Benchiheub, N. Pressure effect on some physical properties of calcium oxide material. *Chem. Phys. Impact*. **7**, 100342. https://doi.org/10.1016/j.chphi.2023.100342 (2023).
40. Benamrani, H., Rekab-Djabri, N., Bouarissa, S. & Daoud Pressure-induced effects on the mechanical and thermophysical properties of $LiAl_2X$ (X = Rh, Pd, Ir and Pt) ternary intermetallic compounds. *Bull. Mater. Sci.* **47** (1), 52. https://doi.org/10.1007/s12034-023-03124-w (2024).
41. Benkara-Mohammed, N., Bioud, N. & Benchiheub, N. Hydrostatic pressure response of semiconducting GaSb applying a semi-empirical approach. *Comput. Condens. Matter*. **39** (2), e00895. https://doi.org/10.1016/j.cocom.2024.e00895 (2024).
42. Bounab, A. M. F. et al. Ab initio study of thermophysical properties of β-PbO_2 under high temperature and pressure. *Theor. Chem. Acc.* **140**, 14. https://doi.org/10.1007/s00214-020-02713-w (2021).
43. Daoud, S., Bouarissa, N., Bioud, N. & Saini, P. K. High-temperature and high-pressure thermophysical properties of AlP semiconducting material: A systematic ab initio study. *Chem. Phys.* **525**, 110399. https://doi.org/10.1016/j.chemphys.2019.110399 (2019).
44. Bioud, N. *Etude des propriétés structurales, élastiques et thermodynamiques des halogénures à base de cuivre, Thèse de doctorat* (Université Ferhat Abbas de Sétif, 2018).
45. Bouferrache, K. et al. Structural, electronic and thermoelectric properties of $CuGe_2P_3$ ternary compound in trigonal phase promising for electronic applications. *Eur. Phys. J. Appl. Phys.* **100**, 29. https://doi.org/10.1051/epjap/2025027 (2025).
46. OztekinCiftci, Y., Bioud, N., Kars, İ. & Durukan Predicting of structural, elastic, vibration and thermodynamic properties of XThSn (X = Pt and Ni) thermoelectric materials. *Phys. Scr.* **100** (1), 015907. https://doi.org/10.1088/1402-4896/ad9529 (2025).
47. Mnisi, B. O., Benecha, M. E. & Tibane, M. M. First-principles study on thermodynamic, structural, mechanical, electronic, and phonon properties of tP16 Ru-based alloys. *Alloys* **3**, 126–139. https://doi.org/10.3390/alloys3020007 (2024).
48. Castillo-Sánchez, J-R. et al. DFT-informed thermodynamic modeling of Al-B with DSC and LIBS-based liquidus validation for boron treatment of aluminum alloys. In R. Seno (ed.), Light Metals, *The Minerals, Metals & Materials Series*. https://doi.org/10.1007/978-3-032-13832-3_161 (2026).

Acknowledgements

The authors would like to acknowledge the Research Center of Basic Sciences, Engineering and High Altitude, Taif University for funding this work.

Author contributions

Conceptualization: A. Benmakhlouf, R. Mezouar, S. Daoud, MA. GhebouliData curation: A. Djemli, Mustafa Jaipallah Abdelmageed Abualreish, Aseel SmeratFormal analysis: S. Alomairy, K. Bouferrache, Murat Yaylac-ıValidation: M. Fatmi.

Declarations

Competing interests

The authors declare no competing interests.

Additional information

Correspondence and requests for materials should be addressed to M.F.

Reprints and permissions information is available at www.nature.com/reprints.

Publisher's note Springer Nature remains neutral with regard to jurisdictional claims in published maps and institutional affiliations.

Open Access This article is licensed under a Creative Commons Attribution-NonCommercial-NoDerivatives 4.0 International License, which permits any non-commercial use, sharing, distribution and reproduction in any medium or format, as long as you give appropriate credit to the original author(s) and the source, provide a link to the Creative Commons licence, and indicate if you modified the licensed material. You do not have permission under this licence to share adapted material derived from this article or parts of it. The images or other third party material in this article are included in the article's Creative Commons licence, unless indicated otherwise in a credit line to the material. If material is not included in the article's Creative Commons licence and your intended use is not permitted by statutory regulation or exceeds the permitted use, you will need to obtain permission directly from the copyright holder. To view a copy of this licence, visit http://creativecommons.org/licenses/by-nc-nd/4.0/.

© The Author(s) 2026